JOURNAL OF MATERIALS SCIENCE 37 (2002) 4993–4998

Characterization of deformation processes in a Zn-22% Al alloy using atomic force microscopy

Y. HUANG, T. G. LANGDON
Departments of Aerospace & Mechanical Engineering and Materials Science, University of Southern California, Los Angeles, CA 90089-1453, USA
E-mail: langdon@usc.edu

The Zn-22% Al eutectoid alloy was subjected to equal-channel angular pressing at a temperature of 473 K to give an as-pressed grain size of ~1.3 μm. Subsequent tensile testing of the as-pressed alloy at room temperature revealed a transition from deformation by a dislocation mechanism at the higher strain rates to superplastic flow at strain rates below $\sim 5 \times 10^{-3}\ s^{-1}$: this corresponds to the transition from region III to region II in conventional superplasticity. Samples were pulled to relatively low total strains, of the order of ~0.2–0.5, and the surface topography was then examined using an atomic force microscope (AFM). The AFM observations confirm the transition in deformation mechanisms with decreasing strain rate and they provide direct evidence for the occurrence of grain boundary sliding within the superplastic regime.

1. Introduction

Equal-channel angular pressing (ECAP) is now established as a useful tool for achieving very substantial grain refinement in bulk materials [1]. Typically, metals processed by ECAP have ultrafine grain sizes lying in the submicrometer range and this grain refinement leads to high strength and a potential for achieving good formability at high temperatures [2, 3]. In ECAP, a sample is pressed through a die contained within a channel which is bent through an angle generally at or close to 90°, thereby introducing a very intense plastic strain into the material. Processing by ECAP was first introduced over 20 years ago by Segal and co-workers in the former Soviet Union [4] and it has now become accepted as a very valuable technique for producing materials having unusual and unique physical and mechanical properties [5].

Numerous reports have been published describing the microstructures and textures produced through ECAP processing [6–8]. Very recently, the approach of microstructural examination was extended by Vinogradov *et al*. [9] in experiments where atomic force microscopy (AFM) was used to study the surface topology of ultrafine-grained Cu and Ni samples after ECAP and subsequent tensile testing. This investigation led to the conclusion that, based on the AFM observations, grain boundary sliding (GBS) occurred in samples subjected to tensile testing at room temperature using a nominal strain rate of $5.6 \times 10^{-4}\ s^{-1}$. However, a review of these results shows that the GBS occurs at exceptionally low temperatures in these materials and this is inconsistent with the well-established observation in high temperature creep that GBS is a diffusion-controlled creep process occurring exclusively at high temperatures, typically above or close to $\sim 0.5\ T_m$, when diffusive processes are reasonably rapid [10], where T_m is defined as the absolute melting point of the material. Since the melting temperatures of Cu and Ni are 1356 and 1723 K, respectively, it follows that room temperature testing corresponds to homologous temperatures of only $\sim 0.22\ T_m$ and $\sim 0.17\ T_m$ and these temperatures are far lower than those generally associated with the advent of GBS. Possible explanations for these results may lie in the very small grain sizes in the as-pressed materials (~200 nm) since it is known that GBS occurs at lower homologous temperatures when the grain size is reduced [11, 12] and/or it may be associated with the enhanced grain boundary diffusivity that may occur in materials processed by ECAP because of the presence of an array of grain boundaries having high-energy non-equilibrium configurations [13].

The present investigation was initiated in order to undertake AFM observations on a material where it is reasonable to anticipate a contribution from GBS in tensile testing at room temperature. The Zn-22% Al eutectoid alloy was chosen for this work for three reasons. First, this alloy is a conventional superplastic material where the mechanical characteristics are well documented [14–16], it is possible to achieve extremely high elongations (>2000%) at elevated temperatures [17, 18] and experiments have shown that GBS makes a very significant contribution to the total strain during superplastic flow [19, 20]. Second, although there are some problems associated with the ECAP processing of the Zn-22% Al alloy because of the tendency for the two separate phases to form agglomerates of ultrafine grains [21], nevertheless a recent report demonstrated that the alloy may be successfully processed to

produce grain sizes down to ~0.6 μm with consequent high superplastic elongations in tensile testing at high temperatures [22]. Third, a recent report demonstrated the successful use of AFM in revealing the microstructural characteristics of Zn-Al coatings on a steel substrate [23].

2. Experimental material and procedures

The experiments were conducted using a commercial Zn-22% Al eutectoid alloy received in a superplastic condition in the form of a plate with a thickness of 25 mm. The initial grain size was measured as ~1.8 μm and there was a duplex microstructure composed of Al-rich and Zn-rich phases. Cylindrically-shaped billets, with a diameter of 10 mm and total lengths of ~6–7 cm, were machined from the plate for ECAP and then annealed for 1 hour at 533 K.

The ECAP processing was conducted using a solid die with an internal channel having a diameter of 10 mm and bent through an angle of 90°: there was also an angle of ~20° at the outer arc of curvature where the two channels intersect. Each sample was pressed at a temperature of 473 K for a total of 8 passes using route B_C where the sample is rotated by 90° in the same sense between each separate pass [24]. It can be shown from first principles that the internal angles associated with the channel lead to an imposed strain close to ~1 on each passage through the die [25], thereby giving a total strain in these samples of ~8.

Following ECAP, tensile specimens were machined from the as-pressed billets with the tensile axes parallel to the pressing direction. Each specimen had a gauge length of 4 mm and a cross-sectional area within the gauge length of 2×3 mm^2. All tensile testing was conducted at room temperature to prevent any surface oxidation or any deterioration of the surface that may interfere with the AFM observations. Initially, tests were conducted to determine the variation of the elongation to failure with the initial strain rate by pulling the tensile specimens to failure over a range of initial strain rates from 10^{-4} to 1 s^{-1} using a testing machine operating at a constant rate of cross-head displacement. Subsequently, the surfaces of some specimens were polished to a mirror-like finish using grinding paper followed by 0.3 and 0.05 μm alumina powder and these specimens were then subjected to interrupted tests where each test was terminated at a selected low elongation.

The AFM observations were performed by cutting the gauge lengths from the polished specimens after tensile testing and using a Digital Instruments Nanoscope III AFM operating in a tapping mode, where the tapping mode was selected in preference to the contact mode to minimize the contact between the AFM tip and the sample.

3. Experimental results

Careful inspection after ECAP revealed an as-pressed grain size of ~1.3 μm: this grain size is a little larger than the grain size of ~0.8 μm reported earlier for the same alloy after 8 passes when the ECAP was performed at a lower temperature of 373 K [22]. Inspection after ECAP showed the grain structure was reasonably homogeneous and the grains were essentially equiaxed.

Fig. 1 shows the results of the tensile testing at room temperature where the true stress σ is plotted against the true strain ε for each separate test. These curves show a region of strain hardening and subsequent strain softening prior to failure for each initial strain rate: similar stress-strain curves have been documented in other materials after ECAP [2, 26]. It is apparent from Fig. 1 that the elongations to failure are reasonably high at the two slowest strain rates and this is illustrated in Fig. 2 where the total elongation is plotted against the initial strain rate. This plot reveals a very clear transition from

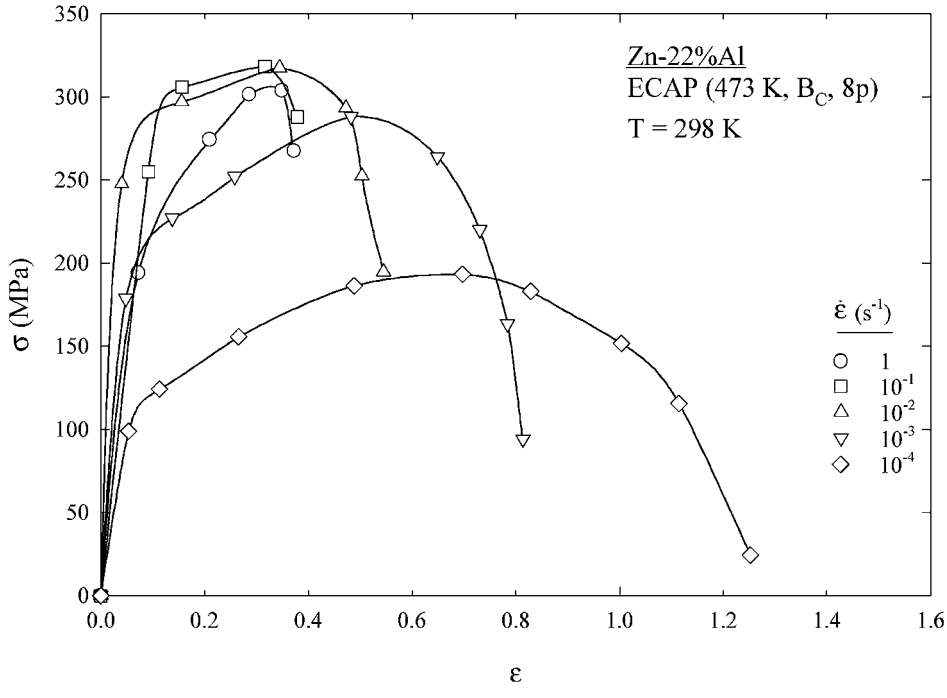

Figure 1 True stress versus true strain in tension for the as-pressed Zn-22%Al alloy at room temperature.

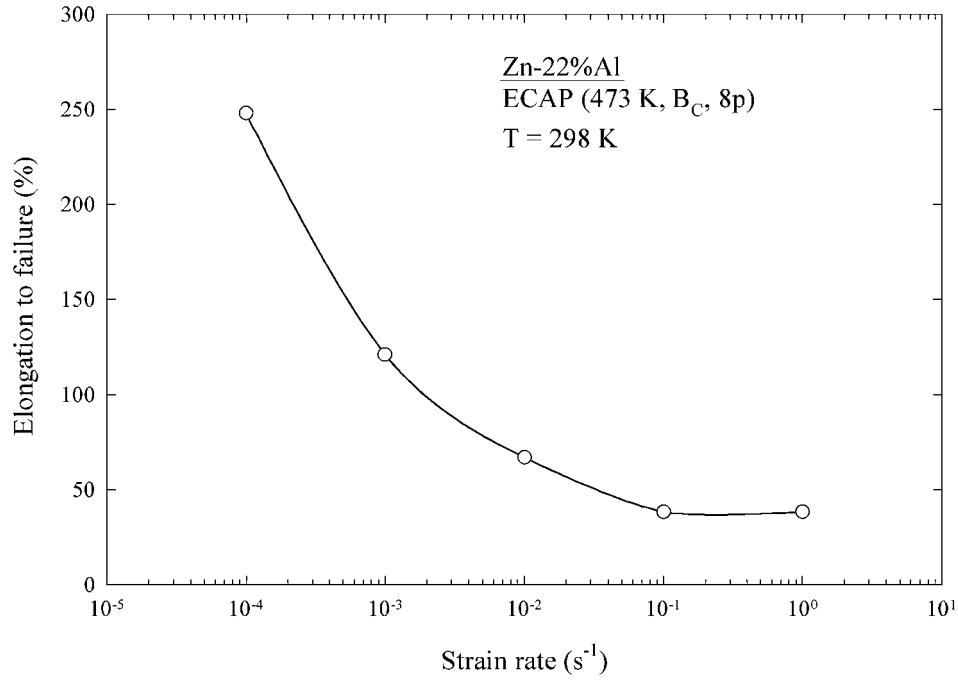

Figure 2 Elongation to failure versus initial strain rate at room temperature showing the transition from the non-superplastic region III at high strain rates to the superplastic region II at strain rates below $\sim 5 \times 10^{-3}\ s^{-1}$.

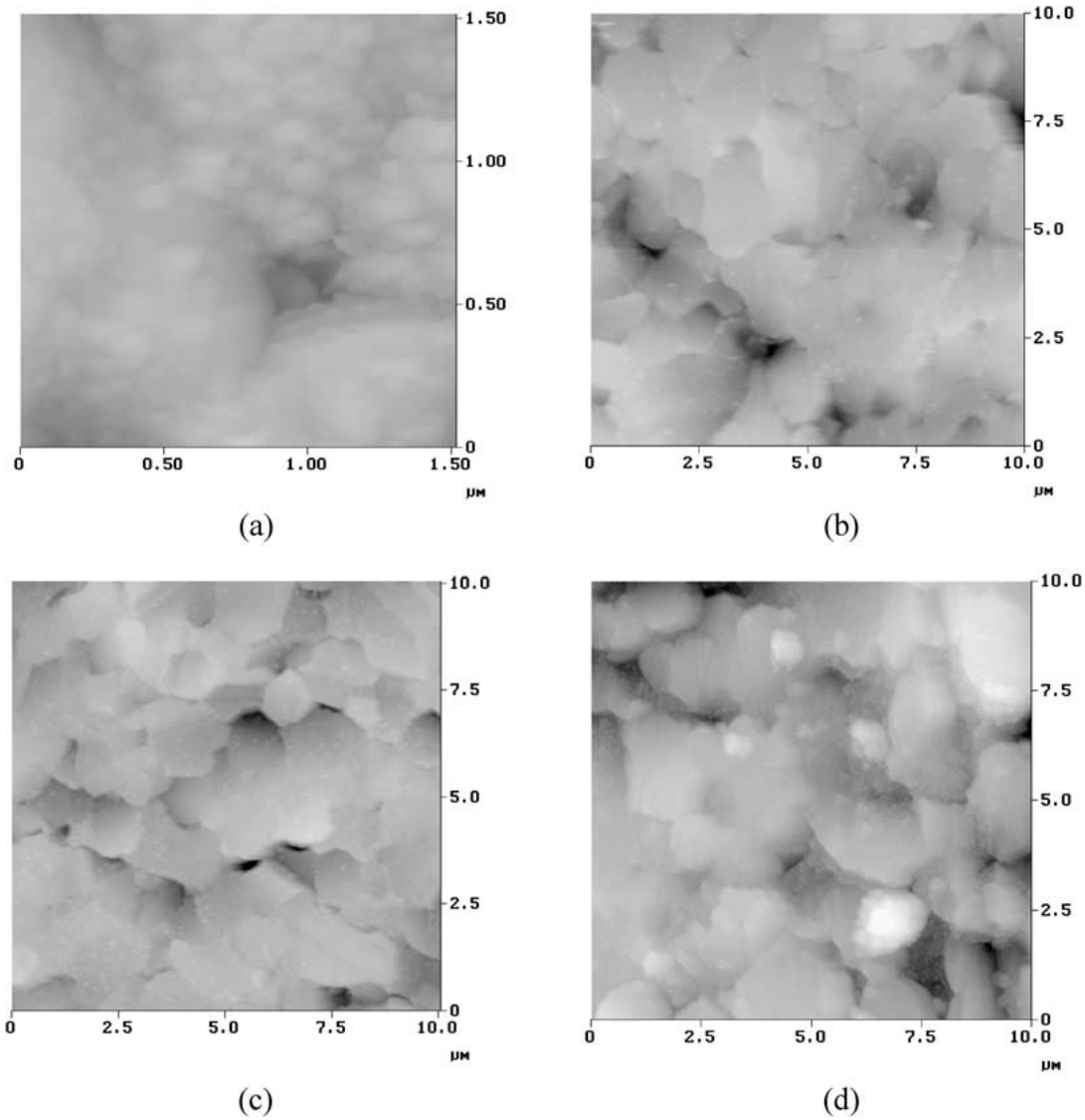

Figure 3 Typical AFM images for samples tested at room temperature at different strain rates: (a) at $10^{-1}\ s^{-1}$ to a strain of 0.17, (b) at $10^{-2}\ s^{-1}$ to a strain of 0.23, (c) at $10^{-3}\ s^{-1}$ to a strain of 0.37 and (d) at $10^{-4}\ s^{-1}$ to a strain of 0.37.

typical behavior in the non-superplastic region III at the faster strain rates to the onset of superplasticity in region II at strain rates below $\sim 5 \times 10^{-3}\ s^{-1}$, where regions III and II represent two of the three characteristic regions of flow in superplastic deformation [27]. It should be noted that an identical effect was reported earlier following testing at room temperature of the Pb-62% Sn eutectic alloy except that the transition to region II occurred at a lower strain rate of $\sim 5 \times 10^{-4}\ s^{-1}$ [28].

The data in Fig. 2 provide a clear demonstration of a transition for the Zn-22% Al alloy from a dislocation process at the faster strain rates to superplastic flow at the lower strain rates. Furthermore, since the strain associated with superplasticity is due almost exclusively to the occurrence of GBS [29], it is apparent that the Zn-22% Al alloy is an excellent material for making use of AFM in a direct comparison of surface topology within and outside of the superplastic regime.

Typical AFM images are displayed in Fig. 3 for samples tested over a range of strain rates: (a) $10^{-1}\ s^{-1}$ to a strain of 0.17 (elongation of 19.1%), (b) $10^{-2}\ s^{-1}$ to a strain of 0.23 (elongation of 25.4%), (c) $10^{-3}\ s^{-1}$ to a strain of 0.37 (elongation of 44.7%) and (d) $10^{-4}\ s^{-1}$ to a strain of 0.37 (elongation of 44.7%). Inspection of Fig. 3 shows the grain boundaries become more distinct with decreasing initial strain rate as the grains emerge from the mirror-like polished surfaces. Thus, these AFM images are consistent with the ductility data in Fig. 2 and confirm the occurrence of GBS at room temperature at the lowest imposed strain rates. By contrast, the grain boundaries remain indistinct at the fastest rate of $10^{-1}\ s^{-1}$ because the contribution from GBS is then insignificant.

There was direct evidence for the occurrence of regular intragranular slip when testing at the faster strain rates especially when testing to reasonably high strains. An example of the occurrence of slip is shown by the AFM image in Fig. 4 for a specimen tested at an initial strain rate of $10^{-3}\ s^{-1}$ to a strain of 0.53, equivalent to an elongation of 69.9%: the upper image shows slip traces in the grain on the right and the lower image shows the three-dimensional surface topography associated with this area of the specimen. By contrast, there was no evidence for any intragranular slip after testing at the slowest strain rates.

The transition from a dislocation deformation process at $10^{-1}\ s^{-1}$ to GBS in superplasticity at $10^{-4}\ s^{-1}$ may be illustrated by examining the three-dimensional surface topographies over an area of $10 \times 10\ \mu m^2$. This is shown in Fig. 5 for the same four samples given in Fig. 3 and ranging through (a) $10^{-1}\ s^{-1}$, (b) $10^{-2}\ s^{-1}$, (c) $10^{-3}\ s^{-1}$ and (d) $10^{-4}\ s^{-1}$. Inspection of these images shows that the individual grains and the steps between these grains become especially evident in Fig. 5d where GBS is dominant.

4. Discussion

The use of atomic force microscopy provides an opportunity to obtain high-resolution images of the surface topography of bulk materials. Thus, AFM is a useful tool for quantifying the nature of deformation in crystalline solids. Although the use of AFM is relatively new, there are several recent reports of AFM investigations exam-

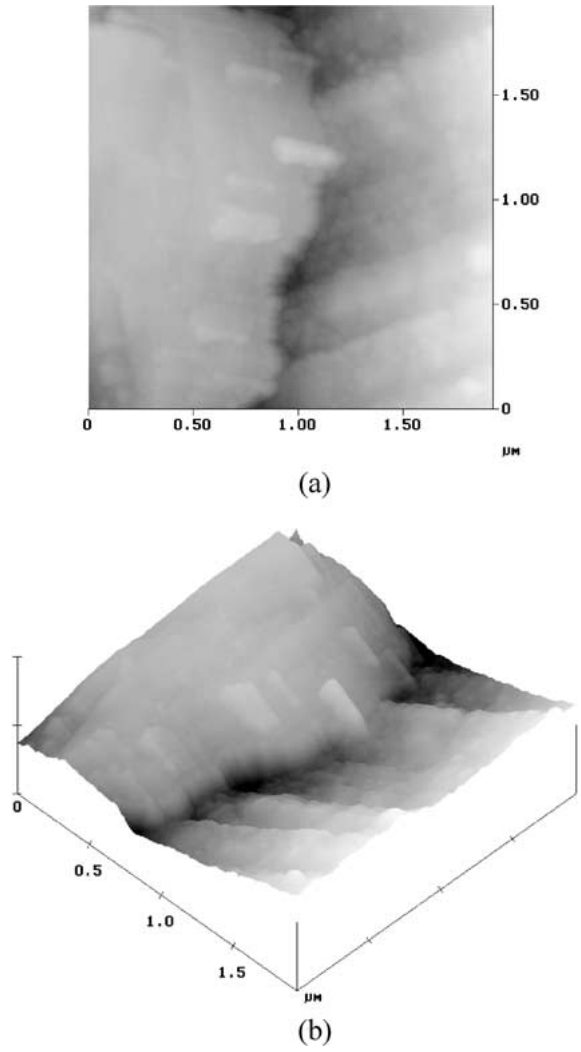

Figure 4 An example of the occurrence of intragranular slip in a specimen tested at an initial strain rate of $10^{-3}\ s^{-1}$ to a strain of 0.53: (a) plan view showing slip in the grain on the right and (b) three-dimensional surface topography of the same area.

ining such features as slip bands and crack initiation in fatigue tests [30–34], the occurrence of diffusion creep in a metal [35] or GBS in ceramics [36, 37], and the nature of surface relief during deformation [38] and nanoindentation [39].

The present results complement the earlier investigation by Vinogradov *et al*. [9] where AFM was used to investigate the deformation behavior of ultrafine-grained samples of Cu and Ni processed by ECAP. By using the superplastic Zn-22% Al eutectoid alloy, the present experiments show that the grain size may be reduced to $\sim 1.3\ \mu m$ after ECAP at a temperature of 473 K and subsequent tensile testing reveals the advent of superplasticity in the conventional region II at strain rates lower than $\sim 5 \times 10^{-3}\ s^{-1}$. The transition from deformation through a dislocation process at the faster strain rates to superplasticity at the slower strain rates is clearly revealed through surface topological observations using AFM.

However, the present results differ in a significant way from those reported by Vinogradov *et al*. [9] where the two pure metals of Cu and Ni were not superplastic, deformation at room temperature corresponded to an homologous temperature of the order of only $\sim 0.2\ T_m$ for both materials, and there was evidence

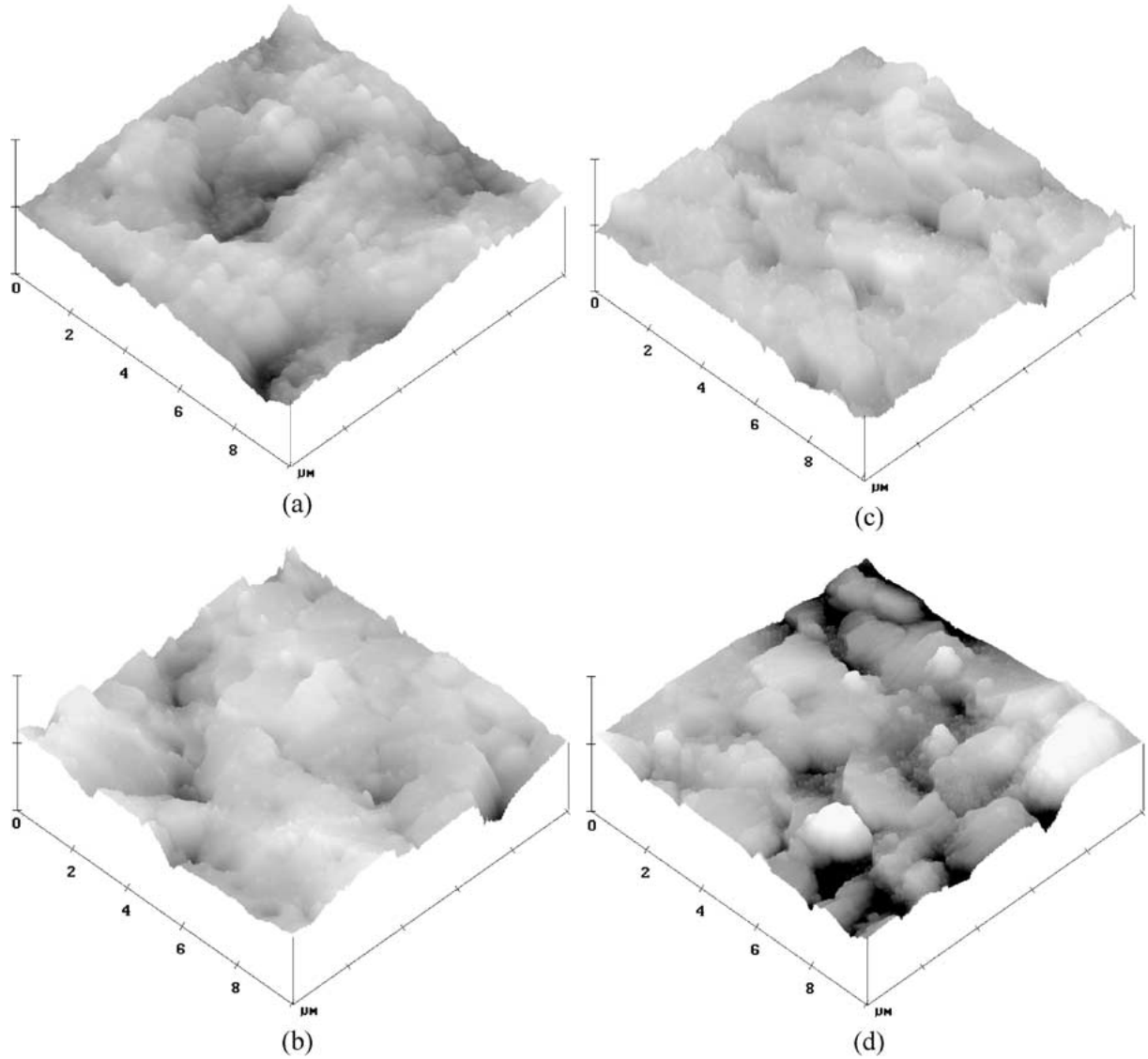

Figure 5 Three-dimensional surface topologies over areas of 10×10 μm^2 for samples tested at room temperature at different strain rates: (a) at 10^{-1} s^{-1} to a strain of 0.17, (b) at 10^{-2} s^{-1} to a strain of 0.23, (c) at 10^{-3} s^{-1} to a strain of 0.37 and (d) at 10^{-4} s^{-1} to a strain of 0.37.

for unusual slip features such as the development of arrays of parallel slip lines or bands oriented at approximately 45° to the loading axis. These slip markings, which were exceptionally long and passed through many of the grains with little or no deviation, were interpreted in terms of a theoretical model developed to account for GBS and the formation of mesoscopic slip planes in nanocrystalline materials with grain sizes up to ∼50 nm [40]. No slip markings of this type were visible on the surface of the Zn-22% Al alloy used in this investigation although the present AFM observations and those of Vinogradov *et al.* [9] were undertaken at comparable total strains. There are two possible reasons for this apparent dichotomy. First, the present results were obtained on an alloy at a reasonably high fraction of the homologous temperature (∼0.4 T_m) so that GBS and superplastic flow was a viable deformation process at room temperature when testing at the lower strain rates. Second, the as-pressed grain size of the Zn-22% Al alloy was larger, by a factor of ∼6, than the grain sizes in the as-pressed Cu and Ni (∼1.3 μm versus ∼200 nm). It is reasonable to anticipate, therefore, that the model developed for the formation of mesoscopic slip planes in nanocrystalline materials is not appropriate for the present alloy.

5. Summary and conclusions

1. Atomic force microscopy was used successfully to examine the surface topological features of a Zn-22% Al eutectoid alloy subjected to ECAP processing and subsequent tensile testing at room temperature.

2. Tensile testing at room temperature revealed a transition from deformation through a dislocation process to deformation by grain boundary sliding and superplasticity at strain rates below $\sim 5 \times 10^{-3}$ s^{-1}. This transition in deformation mechanisms was matched by the AFM observations.

Acknowledgements

This work was supported by the U.S. Army Research Office under Grant No. DAAD19-00-1-0488.

References

1. M. FURUKAWA, Z. HORITA, M. NEMOTO and T. G. LANGDON, *J. Mater. Sci.* **36** (2001) 2835.
2. Z. HORITA, T. FUJINAMI, M. NEMOTO and T. G. LANGDON, *Metall. Mater. Trans.* **31A** (2000) 691.

3. Z. HORITA, M. FURUKAWA, M. NEMOTO, A. J. BARNES and T. G. LANGDON, *Acta Mater.* **48** (2000) 3633.
4. V. M. SEGAL, V. I. REZNIKOV, A. E. DROBYSHEVSKIY and V. I. KOPYLOV, *Russian Metall.* **1** (1981) 99.
5. R. Z. VALIEV, R. K. ISLAMGALIEV and I. V. ALEXANDROV, *Prog. Mater. Sci.* **45** (2000) 103.
6. K. OH-ISHI, Z. HORITA, D. J. SMITH and T. G. LANGDON, *J. Mater. Res.* **16** (2001) 583.
7. A. GHOLINIA, P. BATE and P. B. PRANGNELL, *Acta Mater.* **50** (2002) 2121.
8. S. D. TERHUNE, D. L. SWISHER, K. OH-ISHI, Z. HORITA, T. G. LANGDON and T. R. MCNELLEY, *Metall. Mater. Trans.* **33A** (2002) 2173.
9. A. VINOGRADOV, S. HASHIMOTO, V. PATLAN and K. KITAGAWA, *Mater. Sci. Eng.* A **319–321** (2001) 862.
10. R. C. GIFKINS and T. G. LANGDON, *J. Inst. Metals* **93** (1964/65) 347.
11. R. Z. VALIEV, O. A. KAIBYSHEV, R. I. KUZNETSOV, R. SH. MUSALIMOV and N. K. TSENEV, *Dokl. Akad. Nauk SSR* **301** (1988) 864.
12. S. X. MCFADDEN, R. S. MISHRA, R. Z. VALIEV, A. P. ZHILYAEV and A. K. MUKHERJEE, *Nature* **398** (1999) 684.
13. R. Z. VALIEV, E. V. KOZLOV, YU. F. IVANOV, J. LIAN, A. A. NAZAROV and B. BAUDELET, *Acta Metall. Mater.* **42** (1994) 2467.
14. A. BALL and M. M. HUTCHISON, *Metal Sci. J.* **3** (1969) 1.
15. F. A. MOHAMED and T. G. LANGDON, *Acta Metall.* **23** (1975) 117.
16. F. A. MOHAMED, S.-A. SHEI and T. G. LANGDON, *ibid.* **23** (1975) 1443.
17. H. ISHIKAWA, F. A. MOHAMED and T. G. LANGDON, *Phil. Mag.* **32** (1975) 1269.
18. F. A. MOHAMED, M. M. I. AHMED and T. G. LANGDON, *Metall. Trans.* **8A** (1977) 933.
19. P. SHARIAT, R. B. VASTAVA and T. G. LANGDON, *Acta Metall.* **30** (1982) 285.
20. Z.-R. LIN, A. H. CHOKSHI and T. G. LANGDON, *J. Mater. Sci.* **23** (1988) 2712.
21. M. FURUKAWA, Y. MA, Z. HORITA, M. NEMOTO, R. Z. VALIEV and T. G. LANGDON, *Mater. Sci. Eng.* A **241** (1998) 122.
22. S.-M. LEE and T. G. LANGDON, *Mater. Sci. Forum* **357–359** (2001) 321.
23. F. A. HARDING, N. A. ALARCON and P. G. TOLEDO, *Surf. Rev. Lett.* **8** (2001) 513.
24. M. FURUKAWA, Y. IWAHASHI, Z. HORITA, M. NEMOTO and T. G. LANGDON, *Mater. Sci. Eng.* A **257** (1998) 328.
25. Y. IWAHASHI, J. WANG, Z. HORITA, M. NEMOTO and T. G. LANGDON, *Scripta Mater.* **35** (1996) 143.
26. R. Z. VALIEV, I. V. ALEXANDROV, Y. T. ZHU and T. C. LOWE, *J. Mater. Res.* **17** (2002) 5.
27. T. G. LANGDON, *Metall. Trans.* **13A** (1982) 689.
28. M. M. I. AHMED and T. G. LANGDON, *J. Mater. Sci. Lett.* **2** (1983) 59.
29. T. G. LANGDON, *Mater. Sci. Eng.* A **174** (1994) 225.
30. S. E. HARVEY, P. G. MARSH and W. W. GERBERICH, *Acta Metall. Mater.* **42** (1994) 3493.
31. W. W. GERBERICH, S. E. HARVEY, D. E. KRAMER and J. W. HOEHN, *Acta Mater.* **46** (1998) 5007.
32. L. CRETEGNY and A. SAXENA, *ibid.* **49** (2001) 3755.
33. T. YAMASAKI, Y. KANEKO, H. MIYAMOTO, S. HASHIMOTO and T. MIYAKI, *Mater. Sci. Eng.* A **319–321** (2001) 569.
34. P. VILLECHAISE, L. SABATIER and J. C. GIRARD, *ibid.* **323** (2002) 377.
35. K. R. MCNEE, G. W. GREENWOOD and H. JONES, *Scripta Mater.* **44** (2001) 351.
36. L. CLARISSE, A. BATAILLE, Y. PENNEC, J. CRAMPON and R. DUCLOS, *Ceramics Intl.* **25** (1999) 389.
37. L. CLARISSE, F. PETIT, J. CRAMPON and R. DUCLOS, *ibid.* **26** (2000) 295.
38. N. STANFORD and M. FERRY, *Scripta Mater.* **44** (2001) 941.
39. Y. CHOI, W. Y. CHOO and D. KWON, *ibid.* **45** (2001) 1401.
40. H. HAHN, P. MONDAL and K. A. PADMANABHAN, *Nanostruct. Mater.* **9** (1997) 603.

Received 5 June
and accepted 13 August 2002